Journal of Applied Physics

AIP Publishing

Strain engineering of the transition metal dichalcogenide chalcogen-alloy WSSe

Salvatore Cianci,[1] Elena Blundo,[1] Federico Tuzi,[1] Daniele Cecchetti,[2] Giorgio Pettinari,[2] Marco Felici,[1] and Antonio Polimeni[1]

[1)]*Physics Department, Sapienza Università di Roma, 00185 Rome, Italy*

[2)]*Institute for Photonics and Nanotechnologies, National Research Council, 00133 Rome, Italy*

(*Electronic mail: antonio.polimeni@uniroma1.it)

(*Electronic mail: elena.blundo@uniroma1.it)

(Dated: 29 April 2024)

Alloying has been a powerful and practical strategy to widen the palette of physical properties available to semiconductor materials. Thanks to recent advances in the synthesis of van der Waals semiconductors, this strategy can be extended to monolayers (MLs) of transition metal dichalcogenides (TMDs). Due to their extraordinary flexibility and robustness, strain is another powerful means to engineer the electronic properties of two-dimensional (2D) TMDs. In this article, we combine these two approaches in an exemplary metal dichalcogenide chalcogen-alloy, WSSe. Highly strained WSSe MLs are obtained through the formation of micro-domes filled with high-pressure hydrogen. Such structures are achieved by hydrogen-ion irradiation of the bulk material, a technique successfully employed in TMDs and h-BN. Atomic force microscopy studies of the WSSe ML domes show that the dome morphology can be reproduced in terms of the average of the elastic parameters and adhesion energy of the end compounds WSe_2 and WS_2. Micro-photoluminescence measurements of the WSSe domes demonstrate that the exceedingly high strains ($\varepsilon \sim 4\%$) achieved in the domes trigger a direct-to-indirect exciton transition, similarly to WSe_2 and WS_2. Our findings heighten the prospects of 2D alloys as strain- and composition-engineerable materials for flexible optoelectronics.

INTRODUCTION

The interest for two-dimensional (2D) materials, and in particular for monolayers (MLs) of transition metal dichalcogenides (TMDs), has skyrocketed in the past decade. Thanks to their sizable band gap and strong spin-orbit interactions, 2D semiconducting TMDs have prompted many opportunities for quantum optoelectronics[1] and valleytronics[2] applications, as well as for the observation of interesting physical phenomena like those reported in TMD heterostructures[3]. The all-surface nature of TMD MLs make them especially responsive to mechanical deformations. The latter are an ubiquitous and very often inevitable presence in 2D materials and, at the same time, a precious tool to modify the sample's physical properties[?]. Alloying is also a widely employed and efficacious method to modulate the electronic properties of bulk and nanostructured semiconductors in general[4], and of 2D semiconductors in particular[5]. Thanks to the recent progress in the synthesis of TMD alloys[6–9], these materials are gaining increasing interest since they provide a virtually seamless variation of the properties of an alloyed $MC^{A}_{2x}C^{B}_{2(1-x)}$ ML between the endpoint compounds MC^{A}_{2} and MC^{B}_{2}, where M is a metal, such as Mo and W, and $C^{A,B}$ are chalcogen atoms, such as S, Se and Te[10]. Metal-alloys are also possible, where the varying atomic species is that of the metal atom[11,12]. In $WS_{2x}Se_{2(1-x)}$[13] and $MoS_{2x}Se_{2(1-x)}$[7] alloys, the compositional dependence of the optical gap energy (derived by photoluminescence, PL, measurements) and the vibrational mode frequencies (derived by Raman spectroscopy) show a smooth dependence on x, with a correspondingly small bowing parameter (*i.e.*, small deviation from a linear behaviour)[6,9,14]. A sizable bowing was instead found for metal alloys[6,11,12]. While the band gap and exciton states of TMD alloy MLs (along with information on dark excitons and on the formation of localized excitons acting as quantum emitters) and their vibrational properties have been investigated[6–14], much less is known about the effects of strain on the materials' electronic properties and –on strictly related grounds– about the influence of alloying on the crystal's adhesion energy[15], which is a quantity of uttermost relevance for the processing of TMDs and the fabrication of TMD-based heterostructures.

In this work, we focus on a chalcogen alloy $WS_{2x}Se_{2(1-x)}$ ML with $x \approx 0.5$ (WSSe), subjected to high strain fields. Strain is achieved by exposing WSSe bulk flakes to a low-energy beam of ionized hydrogen that leads to the formation of ML micro-/nano-domes on the flake surface, as previously demonstrated for several TMDs and for hBN[16,17]. The quantitative analysis of the WSSe dome shape permits to show that the elastic parameters and adhesion energy of the WSSe alloy can be evaluated as an average between those of WS_2 and WSe_2. Micro-photoluminescence (μ-PL) measurements, performed also as a function of temperature, reveal the presence of a direct (A)-to-indirect (I) exciton crossover caused by the strain-induced transition of the valence band (VB) maximum from the K to the Γ point of the first Brillouin zone[18]. The energies of the A and I excitons are close to the average values of the A and I excitons observed in WS_2 and WSe_2 domes.

EXPERIMENTAL DETAILS

WSSe thick flakes and MLs were mechanically exfoliated from bulk crystals grown by the flux zone method and purchased from 2D semiconductors. The WSSe alloy compo-

sition was controlled by energy dispersive X-ray analysis (EDX) using a ZEISS-Sigma300 scanning electron microscope (SEM) equipped with an Oxford Instruments X-Act 100 mm energy-dispersive spectrometer. The data were acquired with an acceleration voltage of 28 kV and analysed by the INCA software. The alloy was found to be homogeneous over the whole investigated crystal with a x value of 0.57, see Supplementary Note 1. WS_2 and WSe_2 were purchased from 2D semiconductors and HQ graphene.

Strained MLs in the shape of domes were created by H-ion low-energy ($\sim$ 10 eV) irradiation. Thick (tens to hundreds of layers) flakes of the material were first mechanically exfoliated by the scotch tape method and deposited on SiO_2/Si substrates. The flakes were then mounted in a vacuum chamber, heated to 150°C and exposed to H-ions. As detailed in Ref. 16, protons penetrate through the topmost layer of bulk TMD crystals, leading to the production and accumulation of molecular hydrogen in the first interlayer region. The trapped gas coalesces, leading to the formation of micro/nano-domes made of a ML directly lifted from the underlying bulk crystal and filled with highly pressurized H_2 (tens to hundreds of atm).

The dome morphology was studied by atomic force microscopy (AFM). AFM measurements were performed in tapping mode. We used a Veeco Digital Instruments Dimension D3100 microscope. The microscope uses monolithic silicon probes with a nominal tip curvature radius of 5-10 nm and a force constant of 40 N/m. All the data were analysed with the Gwyddion software and the convolution of the tip used was duly taken into account.

Temperature-dependent μ-PL measurements were performed using a closed-circuit He cryostat by Montana Instruments equipped with x-y nano-positiones by Attocube. The excitation laser was provided by a single frequency Nd:YVO_4 laser (DPSS series by Lasos) emitting at 532 nm. The luminescence signal was spectrally dispersed by a 20.3 cm focal length Isoplane 160 monochromator (Princeton Instruments) equipped with a 150 grooves/mm and a 300 grooves/mm grating and detected by a back-illuminated N_2-cooled Si CCD camera (100BRX by Princeton Instruments). The laser light was filtered out by a very sharp long-pass Razor edge filter (Semrock). A 100$\times$ long-working-distance Zeiss objective with NA = 0.75 was employed to excite and collect the light, in a backscattering configuration and using a confocal setup.

RESULTS

Figure 1 shows the results of the AFM study performed on WSSe domes obtained with a hydrogen dose equal to $d_H = 1.5 \times 10^{16}$ ions/cm^2. Panel (a) displays a 3D AFM map, where large domes coexist with smaller ones. Each dome is characterized by the ratio h_0/R between the maximum height at the dome center (h_0) and the footprint radius (R), see top-right inset in panel (a). In the same inset, the experimental AFM height profile acquired along a diameter of the largest dome (light purple circles) is reproduced by the model (solid black line) presented in Ref. 15 and given by

$$h(r) = h_0 \left[1 - \left(\frac{r}{R}\right)^q\right], \quad (1)$$

with r being the radial coordinate. R, h_0 and q are fitting parameters, with q being generally ≈ 2.2 for TMD domes[15]. Figure 1 (b) shows a statistical analysis of the dome aspect ratio h_0/R. A Gaussian fit to the histogram provides the average value 0.163 ± 0.013 for WSSe domes. This quantity is compared in panel (c) with the values obtained in WS_2 and WSe_2 domes in Ref. 15. Noticeably, the obtained value is closer to the aspect ratio estimated for WS_2 than that estimated for WSe_2.

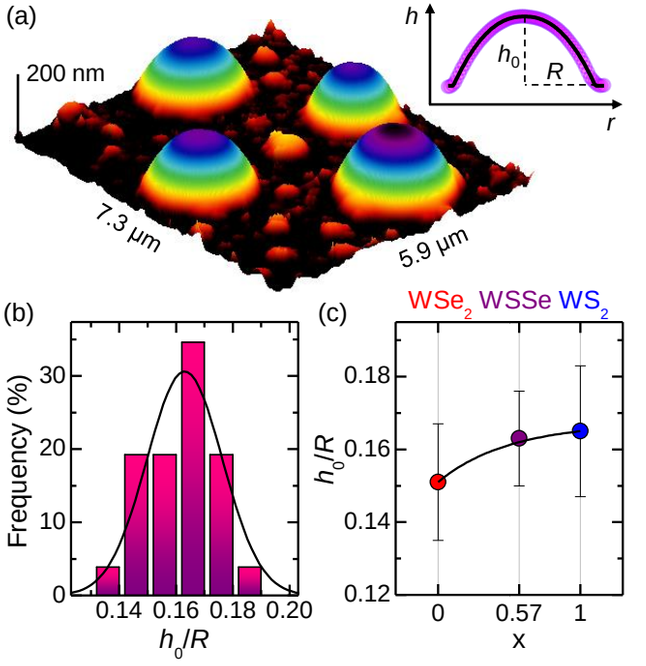

FIG. 1. (a) 3D atomic force microscope (AFM) image of a WSSe showing the formation of domes. Inset: AFM profile taken along the diameter of the largest dome. $h_0 = (198 \pm 2)$ nm, $R = (1.20 \pm 0.02)$ μm, $h_0/R = 0.165 \pm 0.004$. (b) Statistical analysis of the aspect ratio (h_0/R) measured in 27 WSSe domes. A Gaussian fit to the histogram provides an average value of 0.163 ± 0.013. (c) Comparison between the average aspect ratio measured in WSSe and those measured in WSe_2 and WS_2 domes in Ref. 15. As discussed in the main text, the black line is a calculation performed via Eq. 2 by assuming that the elastic parameters and adhesion energy of the alloy scale linearly with x.

This can be rationalized considering that

$$\frac{h_0}{R} = \alpha(\nu) \cdot \left(\frac{\gamma}{E_{2D}}\right)^{1/4}, \quad (2)$$

where $\alpha(\nu)$ is a function of the Poisson's ratio ν (see Ref. 15 for the explicit form), γ is the adhesion energy between the ML and the bulk flake, and E_{2D} is the 2D Young modulus of the ML. For WS_2 and WSe_2, the following parameters were estimated: $\nu_{WS_2} = 0.219$, $\nu_{WSe_2} = 0.196$ (computed theoretically[19,20]), $E_{2D,WS_2} = 162$ N/m, $E_{2D,WSe_2} = 103$

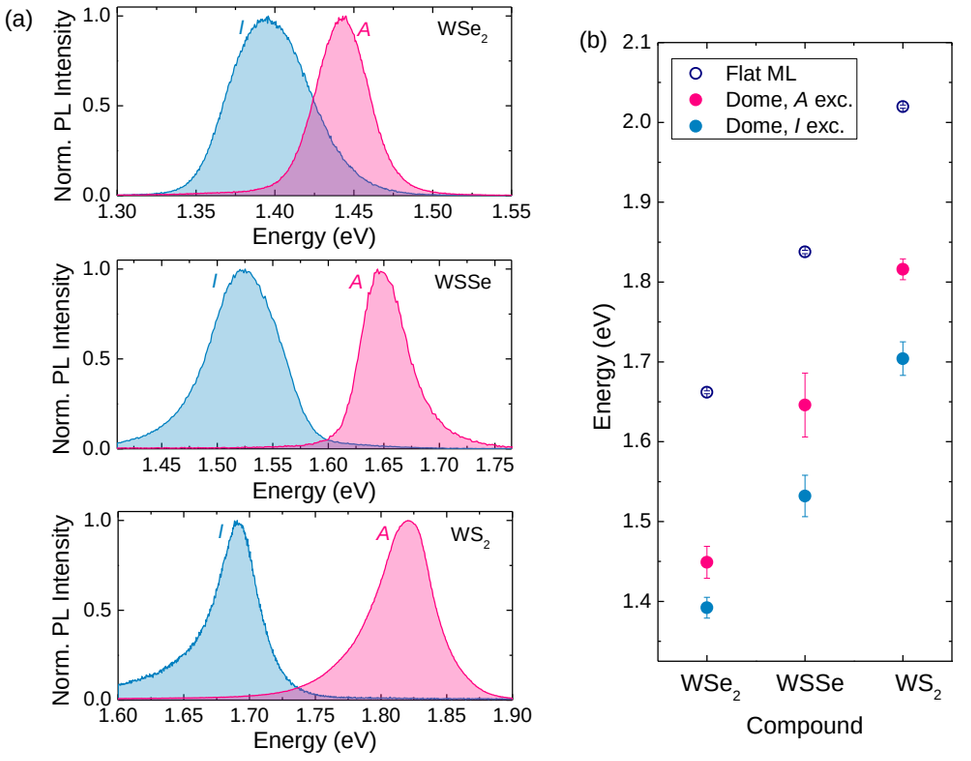

FIG. 2. (a) Room temperature μ-PL spectra of WSe_2, WSSe and WS_2 domes, showing the direct (A) and indirect (I) exciton for all the three compounds. Excitation wavelength equal to 532 nm and laser power equal to 1 μW. (b) Average exciton energy for W-based MLs, compared to their respective A and I exciton energies.

N/m (obtained by an average of the experimentally measured values[15,21–23]), and $\gamma_{WS_2} = (16.8 \pm 7.8)$ meV/Å, $\gamma_{WSe_2} = (6.5 \pm 2.9)$ meV/Å (measured experimentally[15]). If we assume that the elastic parameters and the adhesion energy of WSSe are an average of those of WS_2 and WSe_2, *i.e.*:

$$y_{WSSe} = x \cdot y_{WS_2} + (1-x) \cdot y_{WSe_2} \tag{3}$$

(where $y = \nu, E_{2D}, \gamma$), we would expect the behavior reported in Figure 1(a) as a black line, leading to an average aspect ratio of 0.162 for our WSSe crystal, in excellent agreement with the value measured experimentally. The knowledge of the aspect ratio and elastic parameters is necessary for the quantification of strain. In particular, the maximum strain is achieved at the dome centre, and it is given by:

$$\varepsilon_{tot}^{max} = 2f(\nu) \cdot \left(\frac{h_0}{R}\right)^2 = (3.9 \pm 0.6)\%, \tag{4}$$

where $f(\nu)$ is a function of the Poisson's ratio ν[15] (estimated to be equal to 0.73 for our WSSe crystal). The strain then decreases while going towards the edge (where a strain value $\varepsilon_{tot}^{min} = (1.8 \pm 0.6)\%$ is reached). The high strain values achieved in the domes can affect the optoelectronic properties of the ML significantly[18]. To investigate the effect of strain on the ML, we performed μ-PL measurements. Some exemplary room temperature μ-PL spectra of WSe_2, WSSe and WS_2 domes are displayed in Figure 2 (a). Each panel refers to a different material and displays two spectra obtained by focusing the laser on different regions of the domes. Two recombination bands are observed and indicated as A and I on the high- and low-energy side, respectively. As already reported for the end compounds[18,24], the A band is due to the direct exciton recombination involving an electron and a hole at the K points of the conduction band (K_{CB}) and valence band (K_{VB}), respectively. The I band corresponds to the recombination of the indirect exciton formed by an electron at K_{CB} and a hole at the Γ_{VB} point of the valence band. The latter crosses K_{VB} at sufficiently high strain ($\varepsilon \gtrsim 2.5\%$) thus becoming the topmost valence band. The recombination of the A or I excitons can be evidenced by exciting the edge or the center of the domes, respectively. Indeed, the strain reaches a maximum value of $\varepsilon \sim 4\%$ at the center of the domes, where the direct exciton is at higher energy with respect to the indirect one, which becomes energetically favored and thus dominates the emission spectrum[18]. On the edge of the domes $\varepsilon \sim 2\%$, which is still below the value necessary to change the VB maximum from Γ to K and, therefore, the direct exciton dominates the PL spectrum. It is worth adding that the strain values present in the domes lead to near energy resonant conditions between the A and I excitons[25]. Consequently, the two exciton species admix largely[25] accounting for the sizable oscillator strength (*i.e.*, large PL intensity) retained by the I despite its indirect

character. This is confirmed by time-resolved μ-PL measurements performed on a WSSe dome (see Supplementary Note 2) showing that the *I* band has an overall slightly longer decay time with respect to the *A* band confirming the mixed electronic characteristics of the two excitons.

Figure 2 (b) shows the dependence of the *A* and *I* exciton energy on the dome composition (the energy of the direct *A* exciton of the unstrained ML for the corresponding materials is also displayed as a reference). The values shown in the figure are obtained by an average over different domes and measurements. Like for the elastic parameters discussed before, one may wonder up to what extent the compositional disorder influences the effect of strain on the electronic properties. The data shown in Figure 2 (b) indicate that the energy of the *A* exciton in the domes varies from WSe_2 to WS_2 showing a trend close to that of the direct exciton energy of the strain-free MLs. Furthermore, both the direct and indirect excitons exhibit a similar dependence on the sample composition. These findings indicate that the presence of strain does not alter appreciably the way the electronic properties change upon alloying, thus echoing the results discussed in Figure 1.

The emission properties of the alloyed domes were also studied as a function of temperature. In particular, we investigated the temperature dependence of the μ-PL spectra of two WSSe domes, each characterized by different prevailing exciton transitions. Figure 3 (a) shows the spectra of the two domes recorded with the same exciting laser power of 20 μW and temperature ranging from T=5 K to room temperature (290 K). In one case the indirect *I* exciton is the dominant band (blue line), in the other case only the direct *A* exciton can be observed (red line). This is likely due to different strain values acting on the dome-shaped WSSe ML. Since the direct-to-indirect transition occurs rather sharply as a function of strain[18], domes with different aspect ratio (hence, strain value[15]) may show predominantly one exciton type or the other. Indeed, the dome ensemble is characterized by a distribution of aspect ratios as displayed in Figure 1 (b). Interestingly, Figure 3 (a) shows that in the range from T=5 K to 40 K the spectra of the two domes overlap. As a matter of fact, in this temperature interval the domes deflate due to the liquid phase of H_2 and the PL arises likely from wrinkled WSSe MLs. However, when T increases, liquid H_2 turns gas and strain establishes again quickly. The center of mass of the spectrum is shown in Figure 3 (b) for both domes. In the dome displaying the indirect transition, one can notice a faster thermal shift of the emission band as compared to that of the other dome, where the direct exciton dominates. This behaviour arises from the nearly double (negative) shift rate induced by the strain in the indirect band gap energy with respect to the strain shift rate of the direct band gap, as previously reported[18,26–28]. Indeed, as the temperature increases, H_2 expands and transfers an increasingly larger amount of strain to the ML dome[29]. In turn, this extra strain adds to the thermal shift of the band gap of the *I* exciton in a more relevant manner than for the *A* exciton. Eventually, at room temperature the two exciton bands differ by about 150 meV, similar the data shown in Figure 2 (b).

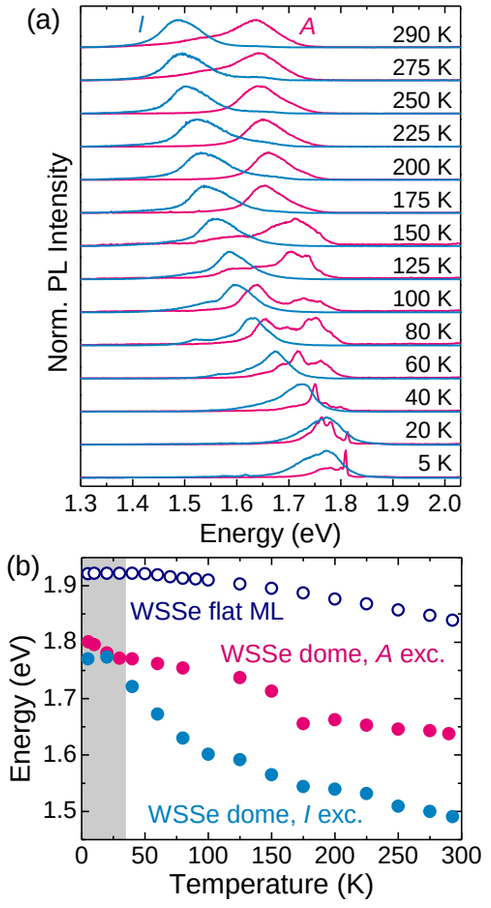

FIG. 3. (a) PL spectra as a function of temperature of two WSSe domes displaying the indirect (*I*) exciton and direct (*A*) exciton. Excitation wavelength equal to 532 nm, and laser power equal to 20 μW. (b) *I* and *A* exciton energy for the two domes of panel (a), and comparison with the *A* exciton behavior in an unstrained flat WSSe ML.

CONCLUSIONS

In this work, we investigated the combined action of alloying and strain in WSSe and compared the effects observed therein with those of the end compounds WSe_2 and WS_2. To this end we studied the elastic and electronic properties of ML domes fabricated by H-ion irradiation. The domes turn out to be a practical and effective means to address up to what extent the mechanical deformations alter the way the elastic and electronic properties of TMD chalcogen-alloy MLs change with composition. Our results indicate that strain and composition combine in a "linear" manner and together widen considerably the range of tunability of the mechanical and electronic properties of TMD alloys. Such tunability could be exploited, *e.g.*, for the design of TMD-based mechanical resonators[30] with tailored characteristics, or for the achievement of strain- and composition-engineered quantum emitters[10,29,31] emitting at specific wavelengths.

SUPPLEMENTARY MATERIAL

The Supplementary Material reports the elemental analysis of the WSSe crystal investigated (Supplementary Note 1) and time-resolved μ-PL measurements of a WSSe dome (Supplementary Note 2).

ACKNOWLEDGMENTS

A.P. and M.F. acknowledge financial support from the PNRR MUR project PE0000023-NQSTI. This project was partly funded within the QuantERA II Programme that has received funding from the European Union's Horizon 2020 research and innovation programme under Grant Agreement No 101017733, and with funding organisations Ministero dell'Universitá e della Ricerca (A.P and M.F.) and by Consiglio Nazionale delle Ricerche (G.P. and D.C.).

DATA AVAILABILITY STATEMENT

The data that support the findings of this study are available from the corresponding author upon reasonable request.

[1] X. Li, L. Tao, Z. Chen, H. Fang, X. Li, X. Wang, J.-B. Xu, and H. Zhu, "Graphene and related two-dimensional materials: Structure-property relationships for electronics and optoelectronics," Appl. Phys. Rev. **4**, 021306 (2017).
[2] Y. Liu, Y. Gao, S. Zhang, J. He, J. Yu, and Z. Liu, "Valleytronics in transition metal dichalcogenides materials," Nano Res. **12**, 2695 (2019).
[3] L. Du, M. R. Molas, Z. Huang, G. Zhang, F. Wang, and Z. Sun, "Moiré photonics and optoelectronics," Science **379**, eadg0014 (2023).
[4] S. Adachi, *Properties of Semiconductor Alloys: Group-IV, III-V and II-VI Semiconductors* (John Wiley and Sons, Hoboken, New Jersey (2009)).
[5] A. Silva, J. Cao, T. Polcar, and D. Kramer, "Design guidelines for two-dimensional transition metal dichalcogenide alloys," Chem. Mater. **34**, 10279 (2022).
[6] Z. Liu, S. Y. Tee, G. Guan, and M.-Y. Han, "Atomically substitutional engineering of transition metal dichalcogenide layers for enhancing tailored properties and superior applications," Nanomicro Lett. **16**, 95 (2024).
[7] A. Silva, J. Cao, T. Polcar, and D. Kramer, "Rapid wafer-scale growth of $MoS_{2(1-x)}Se_{2x}$ alloy monolayers with tunable compositions and optical properties for high-performance photodetectors," ACS Appl. Nano Mater. **4**, 12609 (2021).
[8] R. Li, J. Yu, B. Yao, X. Huang, Z. Fu, Z. Zhou, G. Yuan, J. Xu, and L. Gao, "Controllable growth of wafer-scale monolayer transition metal dichalcogenides ternary alloys with tunable band gap," Nanotechnology **34**, 075603 (2022).
[9] Y. Zhao, Z. Zhang, and G. Ouyang, "Band shift of 2D transition-metal dichalcogenide alloys: size and composition effects," Appl. Phys. A **124**, 1432 (2018).
[10] K. Olkowska-Pucko, E. Blundo, N. Zawadzka, S. Cianci, D. Vaclavkova, P. Kapuściński, D. Jana, G. Pettinari, M. Felici, K. Nogajewski, M. Bartoš, K. Watanabe, T. Taniguchi, C. Faugeras, M. Potemski, A. Babiński, A. Polimeni, and M. R. Molas, "Excitons and trions in WSSe monolayers," 2D Materials **10**, 015018 (2023).
[11] J. Park, M. S. Kim, B. Park, S. H. Oh, S. Roy, J. Kim, and W. Choi, "Composition-tunable synthesis of large-scale $Mo_{(1-x)}W_xS_2$ alloys with enhanced photoluminescence," ACS Nano **12**, 6301 (2018).
[12] Y. Chen, J. Xi, D. O. Dumcenco, Z. Liu, K. Suenaga, D. Wang, Z. Shuai, Y.-S. Huang, , and L. Xie, "Tunable band gap photoluminescence from atomically thin transition-metal dichalcogenide alloys," ACS Nano **7**, 4610 (2013).
[13] X. Duan, C. Wang, Z. Fan, G. Hao, L. Kou, U. Halim, H. Li, X. Wu, Y. Wang, J. Jiang, A. Pan, Y. Huang, R. Yu, and X. Duan, "Synthesis of $WS_{2x}Se_{2-2x}$ alloy nanosheets with composition-tunable electronic properties," Nano Lett. **16**, 264 (2016).
[14] F. A. Nugera, P. K. Sahoo, Y. Xin, S. Ambardar, D. V. Voronine, U. J. Kim, Y. Han, H. Son, and H. R. Gutiérrez, "Bandgap engineering in 2D lateral heterostructures of transition metal dichalcogenides via controlled alloying," Small **18**, 2106600 (2022).
[15] E. Blundo, T. Yildirim, G. Pettinari, and A. Polimeni, "Experimental adhesion energy in van der Waals crystals and heterostructures from atomically thin bubbles," Phys. Rev. Lett. **127**, 046101 (2021).
[16] D. Tedeschi, E. Blundo, M. Felici, G. Pettinari, B. Liu, T. Yildrim, E. Petroni, C. Zhang, Y. Zhu, S. Sennato, Y. Lu, and A. Polimeni, "Controlled micro/nanodome formation in proton-irradiated bulk transition-metal dichalcogenides," Adv. Mater. **31**, 1903795 (2019).
[17] E. Blundo, A. Surrente, D. Spirito, G. Pettinari, T. Yildirim, C. A. Chavarin, L. Baldassarre, M. Felici, and A. Polimeni, "Vibrational properties in highly strained hexagonal boron nitride bubbles," Nano Lett. **22**, 1525 (2022).
[18] E. Blundo, M. Felici, T. Yildirim, G. Pettinari, D. Tedeschi, A. Miriametro, B. Liu, W. Ma, Y. Lu, and A. Polimeni, "Evidence of the direct-to-indirect band gap transition in strained two-dimensional WS_2 and MoS_2, and WSe_2," Phys. Rev. Res. **2**, 012024 (2020).
[19] M. de Jong, W. Chen, T. Angsten, A. Jain, R. Notestine, A. Gamst, M. Sluiter, C. K. Ande, S. van der Zwaag, J. J. Plata, C. Toher, S. Curtarolo, G. Ceder, K. A. Persson, and M. Asta, "Charting the complete elastic properties of inorganic crystalline compounds," Sci. Data **2**, 150009 (2015).
[20] A. Jain, S. P. Ong, G. Hautier, W. Chen, W. D. Richards, S. Dacek, S. Cholia, D. Gunter, D. Skinner, G. Ceder, and K. A. Persson, "Commentary: The Materials Project: A materials genome approach to accelerating materials innovation," APL Mater. **1**, 011002 (2013).
[21] K. Liu, Q. Yan, M. Chen, W. Fan, Y. Sun, J. Suh, D. Fu, S. Lee, J. Zhou, S. Tongay, J. Ji, J. B. Neaton, and J. Wu, "Elastic properties of chemical-vapor-deposited monolayer MoS_2, WS_2, and their bilayer heterostructures," Nano Lett. **14**, 5097–5103 (2014).
[22] N. Iguiñiz, R. Frisenda, R. Bratschitsch, and A. Castellanos-Gomez, "Revisiting the buckling metrology method to determine the young's modulus of 2d materials," Adv. Mater. **31**, 1807150 (2019).
[23] R. Zhang, V. Koutsos, and R. Cheung, "Elastic properties of suspended multilayer WSe_2," Appl. Phys. Lett. **108**, 042104 (2016).
[24] E. Blundo, E. Cappelluti, M. Felici, G. Pettinari, and A. Polimeni, "Strain-tuning of the electronic, optical, and vibrational properties of two-dimensional crystals," Appl. Phys. Rev. **8**, 021318 (2021).
[25] E. Blundo, P. E. Faria Junior, A. Surrente, G. Pettinari, M. A. Prosnikov, K. Olkowska-Pucko, K. Zollner, T. Woźniak, A. Chaves, T. Kazimierczuk, M. Felici, A. Babiński, M. R. Molas, P. C. M. Christianen, and J. F. A. Polimeni, "Strain-induced exciton hybridization in WS_2 monolayers unveiled by Zeeman-splitting measurements," Phys. Rev. Lett. **129**, 067402 (2022).
[26] H. Shi, H. Pan, Y.-W. Zhang, and B. I. Yakobson, "Quasiparticle band structures and optical properties of strained monolayer MoS_2 and WS_2," Phys. Rev. B **87**, 155304 (2013).
[27] C.-H. Chang, X. Fan, S.-H. Lin, and J.-L. Kuo, "Orbital analysis of electronic structure and phonon dispersion in MoS_2, $MoSe_2$, WS_2, and WSe_2 monolayers under strain," Phys. Rev. B **88**, 195420 (2013).
[28] K. Zollner, P. E. F. Junior, and J. Fabian, "Strain-tunable orbital, spin-orbit, and optical properties of monolayer transition-metal dichalcogenides," Phys. Rev. B **100**, 195126 (2019).
[29] S. Cianci, E. Blundo, F. Tuzi, G. Pettinari, K. Olkowska-Pucko, E. Parmenopoulou, D. B. Peeters, A. Miriametro, T. Taniguchi, K. Watanabe, A. Babinski, M. R. Molas, M. Felici, and A. Polimeni, "Tailoring the optical properties of 2d transition metal dichalcogenides by strain," Adv. Optical Mater. **11**, 2202953 (2023).
[30] T. Yildirim, L. Zhang, G. P. Neupane, S. Chen, J. Zhang, H. Yan, M. M. Hasan, G. Yoshikawa, and Y. Lu, "Towards future physics and applications via two-dimensional material NEMS resonators," Nanoscale **12**, 22366–22385 (2020).
[31] G. D. Shepard, O. A. Ajayi, X. Li, X.-Y. Zhu, J. Hone, and S. Strauf, "Nanobubble induced formation of quantum emitters in monolayer semiconductors," 2D Materials **4**, 021019 (2017).